Simulation and test of an agricultural unmanned airboat maneuverability model

Yufei Liu[1], Noboru Noguchi[2*], Roshanian Fard Ali[1]

(1. *Graduate School of Agriculture, Hokkaido University, Kita-9, Kita-ku, Sapporo, Hokkaido 060-8589, Japan*;
2. *Research Faculty of Agriculture, Hokkaido University, Kita-9, Kita-ku, Sapporo, Hokkaido 060-8589, Japan*)

Abstract: The objective of this research was to determine the Nomoto model maneuverability indices of an agricultural unmanned airboat which was developed to perform autonomous weeding and paddy growth monitoring in a paddy field. A global positioning system compass and an inertial measurement unit were attached on the airboat body to record the position, heading and angular rate. The zig-zag experiments were adopted to obtain the maneuverability indices. The Matlab-based maneuvering simulations were conducted and compared with field experimental data of circular motion test and sinusoidal running test, respectively. The results showed that the trace error was at sub-meter level, which expounds the validity of the obtained maneuvering indices. The proposed Nomoto model maneuverability indices can be used to improve the airboat precise automatic control in paddy field.

Keywords: Nomoto model, unmanned airboat, maneuvering simulation, GPS compass, IMU
DOI: 10.3965/j.ijabe.20171001.2538

Citation: Liu Y F, Noguchi N, Ali R F. Simulation and test of an agricultural unmanned airboat maneuverability model. Int J Agric & Biol Eng, 2017; 10(1): 88–96.

1 Introduction

Airboat is a flat-bottomed vessel that is propelled by an aircraft-type propeller and powered by either an electromotor or an automotive engine. The airboat depends primarily on air thrust for propulsion[1]. Normally, the airboat is made of three main parts: an air propeller, a rudder and a hull. The propeller produces a column of air as propulsive force. The rudder deviates the air column to produce steering force. The hull is a platform that keeps those two parts out of the water surface. Since both the motor and the propeller are not under water, the airboat has an obvious low draft feature. Hence, the airboat is very suitable for running in shallow water or swamps[2]. Up to now, the airboat has been improved immensely and applied in many fields, such as eco-tourism, environment monitor and emergency rescue[3-7].

Paddy rice is a semi-aquatic plant, its growth is strongly influenced by water supply. The depth of water is around 100 mm especially in the early stage of paddy growth[8]. Various farming tasks including fertilizing and weeding are also conducted in this stage. However, because the line spacing of paddy is normally 25-30 cm in the paddy field[9], it is difficult to drive a wheel-type tractor or a crawler-type tractor, the soil and paddy seedlings will be easily damaged by tractors unless to leave some wide farm tracks in the paddy field, which wastes planting area. Another way is relying on manual power, which is inefficient and has a heavy labor intensity. But the airboat could be used instead of tractors or the farmers to do farm work in paddy fields and is not necessary to worry about damaging the paddy seedlings. Therefore, for large-scale intensive production,

Received date: 2016-04-18 **Accepted date:** 2016-10-11
Biographies: Yufei Liu, PhD student, research interests: agricultural robots, Email: liu@bpe.agr.hokudai.ac.jp; **Roshanian Fard Ali**, PhD student, research interests: agricultural machine design, Email: alirf@bpe.agr.hokudai.ac.jp.
***Corresponding author: Noboru Noguchi**, PhD, Professor, research interests: agricultural robots. Mailing address: Research Faculty of Agriculture, Hokkaido University, Sapporo, 060-8589, Japan. Email: noguchi@bpe.agr.hokudai.ac.jp.

there is a demand to develop an agricultural unmanned airboat that can run autonomously in the paddy field to fertilize and weed before paddy transplanting and during the paddy early growth stage.

Modeling and control are two crucial parts for achieving airboat automation. Furthermore, modeling is the basis of precise automatic control of heading-keeping and course-keeping. The boat maneuverability is defined as the dynamic performance required to keep or change the boat speed, heading and position under certain force. To describe the maneuverability, a mechanical model was used, which follows Newton's law of motion. Abkowitz model[10] and Maneuvering Modeling Group (MMG) model[11] were used to analyze the stress on the boat. These models have explicit physical meaning, but mostly rely on complicated equipment to conduct the captive model test, such as oblique towing test[12] and rotating arm test[13]. Another model, Nomoto model, is a response model. This model describes the dynamic relationship between the rudder deflection and the airboat turning angular rate[14]. It is a simple structure to directly respond to the rudder effect.

The objective of this research was to determine the Nomoto model maneuverability indices of an agricultural airboat used in a paddy field. The maneuverability indices, turning index and following index were obtained by using zig-zag experiments. Computer simulation was carried out to verify the feasible maneuverability indices by using Matlab software. Finally, the field experiments including circular turning and sinusoidal running were conducted by using the Nomoto model with the obtained turning index and following index. At the end of the paper, the influence of crosswind force on airboat is preliminarily analyzed. It gives a meaningful way to improve the control accuracy in the future work.

2 Materials and methods

2.1 Airboat setup

The modified agriculture airboat[15] used in this study is shown in Figure 1. For remote control and realizing unmanned farm work in paddy field, the airboat was developed into two parts, one part on the airboat body and the other part on the embankment. Figure 2 shows the structure of the modified airboat hardware system. The attached sensors, like GPS compass (V100, Hemisphere)[16], magnetic sensor (GV-101, FUTABA) and inertial measurement unit (IMU) (VN-100, VectorNav Technologies)[17], were used for obtaining the parameters of airboat running situation. The processors, onboard computer (DN2800MT, Intel) and developed Arduino microcontroller board (UNO, Arduino) based electronic control unit (ECU), were applied for data processing. The local WIFI network environment was built by a powerful wireless router (WXR-2533DHP, Buffalo)[18]. The airboat can be monitored and controlled using wireless communication. Further implementation details of the modified airboat were described in reference [19].

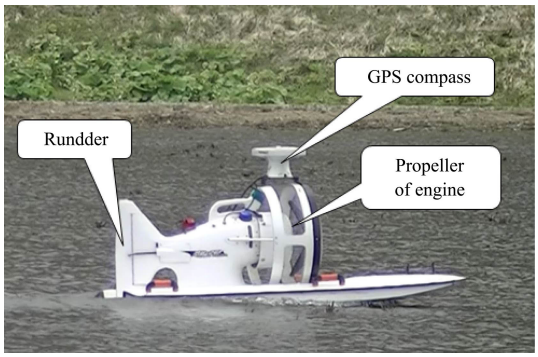

Figure 1 Agricultural unmanned airboat

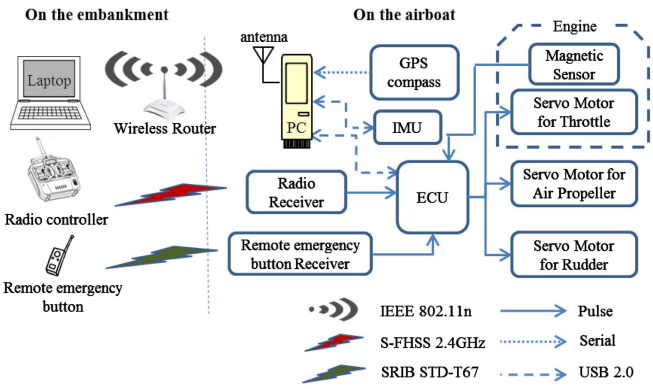

Figure 2 Block diagram of the modified airboat hardware system

2.2 Mathematical model analysis

The traditional underwater propeller providing propulsive force cannot be used in a paddy field. It will damage the paddy seedlings and the airboat will be stranded. An air propeller is therefore necessary for providing maneuvering power. A column of air flow produced by the air propeller produces forward momentum for the airboat to move on water. Regardless of whether the vehicle is an airboat or an

underwater vehicle, under the condition of disturbance by wind, waves and water flow, the vehicle motion is regarded as a 6-degree of freedom (6-DOF) rigid body motion in space. According to the naming system proposed by the Society of Naval Architects & Marine Engineers (SNAME), the three translational motions are surge, sway and heave, the three rotational motions are roll, pitch and yaw. Figure 3 ashows the 6-DOF motion of the airboat in a geodetic coordinate system. To determine the equations of motion, two reference coordinate systems were created. As well as the geodetic coordinate system, an airboat body-fixed coordinate system was created. The motion state of the vehicle can be uniquely identified by the two coordinate systems. The transformational relation between the two coordinate systems is given by Equation (1):

$$\dot{\eta} = J(\phi,\theta,\psi)v \tag{1}$$

where, $\dot{\eta}$ is the first order derivative of the position vector in the geodetic coordinate system; J is the transformational matrix related to the Euler angles as expressed in Equation (2), where ϕ denotes roll, θ denotes pitch, and ψ denotes yaw, rad; v is the linear velocity vector in the body-fixed coordinate system.

$$J = \begin{bmatrix} \cos(\psi)\cos(\theta) & -\sin(\psi)\cos(\phi)+\sin(\phi)\sin(\theta)\cos(\psi) & \sin(\psi)\sin(\phi)+\sin(\theta)\cos(\psi)\cos(\phi) \\ \sin(\psi)\cos(\theta) & \cos(\psi)\cos(\phi)+\sin(\phi)\sin(\theta)\sin(\psi) & -\cos(\psi)\sin(\phi)+\sin(\theta)\sin(\psi)\cos(\phi) \\ -\sin(\theta) & \sin(\phi)\cos(\theta) & \cos(\phi)\cos(\theta) \end{bmatrix} \tag{2}$$

In a paddy field where the water is less than 10 cm deep in normal conditions, the effects of water flow and water waves can be ignored after irrigation. In other words, the pitching and rolling of the airboat are very small when the airboat moves in a paddy field and therefore can be neglected. Hence, for the convenience of discussion, the motions of the vehicle in heave direction, pitch direction and roll direction can also be neglected. Only the horizontal motion control was utilized, which means only surge, sway and yaw were considered. Figure 3b shows the relation between force and moments of the airboat in the horizontal coordinate system. The origin point of the body-fixed coordinate x-o-y was assumed to be at the centre of gravity of the airboat, Euler's motion equations given as Equation (3) can describe the control motion modelling.

$$\begin{cases} F_x(u,v,r,,\dot{u},\dot{v},\dot{r}) = m(\dot{u}-vr) \\ F_y(u,v,r,\dot{u},\dot{v},\dot{r}) = m(\dot{v}+ur) \\ M_z(u,v,r,\dot{u},\dot{v},\dot{r}) = I_z\dot{r} \end{cases} \tag{3}$$

where, F_x is the resultant force acting in the surge x direction, N; F_y represents the resultant force acting in the sway y direction, N; M_z is the moment of the airboat with respect to the yaw rate r direction, N·m; m is the weight of the airboat, kg; u is velocity in the x direction, m/s; v is lateral velocity in the y direction, m/s; r is rotation speed, rad/s; I_z is the moment of inertia with respect to the yaw direction, kg·m^2; $\dot{u}$, $\dot{v}$ and $\dot{r}$ are the first time derivatives of u, v and r as the accelerations, respectively.

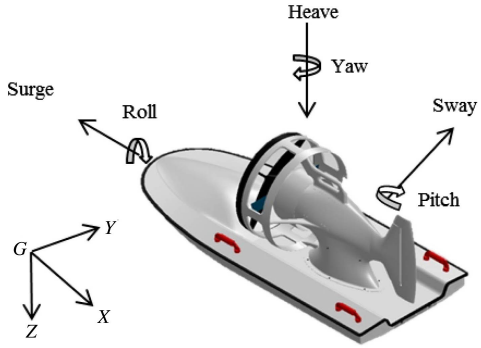

a. 6-DOF motion of the airboat in geodetic coordinate system

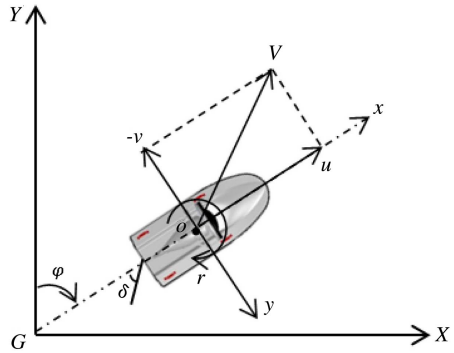

b. 3-DOF motion of the airboat in horizontal coordinate system

Figure 3 Motion of the airboat in diffirent coordinates

Linearization of Equation (3) is appropriate for a constant speed and straight line motion condition. The transfer function between the rudder angle δ and the yaw rate r of an airboat can be described by the linear 2nd order model of Nomoto written as Equation (4):

$$\frac{r(s)}{\delta(s)} = \frac{K(1+T_3 s)}{(1+T_1 s)(1+T_2 s)} \tag{4}$$

where, K is the rudder gain constant; s is used to denote the Laplace operator; T_i (i=1,2,3) are three time constants.

A 1st order approximation equation is obtained by Equation (5):

$$\frac{r(s)}{\delta(s)}=\frac{K}{(1+Ts)} \tag{5}$$

where, $T=T_1+T_2-T_3$ is the effective time constant.

The heading angle φ is related to the yaw rate r as Equation (6):

$$\dot{\varphi}(t)=r(t) \tag{6}$$

Then, by combining Equation (5) and Equation (6), the 1st order Nomoto model function can be written as Equation (7):

$$\frac{\varphi(s)}{\delta(s)}=\frac{K}{s(1+Ts)} \tag{7}$$

Through Laplace transform, Equation (7) can be expressed as Equation (8) in time domain.

$$T\ddot{\varphi}+\dot{\varphi}=K\delta \tag{8}$$

where, $\ddot{\varphi}$ is yaw angular acceleration, rad/s^2; $\dot{\varphi}$ is yaw rate, rad/s.

At the initial conditions of t_0=0, r_0=0, $\delta=\delta_0$, the solution of Equation (8) can be written as Equation (9):

$$r(t)=K\delta_0(1-e^{-t/T}) \tag{9}$$

The solution shows that yaw rate r increases exponentially and approaches to a constant value $K\delta_0$ over time. The yaw rate r is related to the rudder angle δ with respect to the Nomoto model indices of K and T.

The heading angle φ can therefore be obtained by angular rate r via an integral as Equation (10):

$$\varphi(t)=\int r(t)dt=K\delta_0(t-T+Te^{-t/T}) \tag{10}$$

In horizontal coordinate system, assuming that the airboat is at the position (x_0, y_0) in time t_0, steering rudder from time t_0, the position (x_t, y_t) can be described by Equation (11) and (12):

$$x_{t+1}=x_t+(u_t\sin\varphi_t-v_t\cos\varphi_t)\Delta t \tag{11}$$

$$y_{t+1}=y_t+(u_t\cos\varphi_t+v_t\sin\varphi_t)\Delta t \tag{12}$$

On the condition of knowing Nomoto model indices of K and T, the arbitrary position of the airboat can be predicted by combining Equations (10)-(12).

2.3 Identification of *K* and *T*

For obtaining the indices K and T, it is necessary to conduct zig-zag manoeuvring test. At the beginning, the boat should be kept into a uniform motion in a straight course, then, the rudder be reversed alternately by an angle δ to either side at a heading angle φ (normally, $\varphi=\delta$) from the initial course. Figure 4 shows the characteristic curve of zig-zag manoeuvring test. The rudder turns to right side at first execution. When the heading φ is over the angle δ, the rudder is reversed to $-\delta$ on the left side. After turning the rudder, the airboat initially continues turning on the right side with decreasing yaw rate until it becomes negative. The airboat finally turns to the left side in response to the rudder angle $-\delta$. When the heading φ is over the angle $-\delta$, the rudder is reversed again to the right side with the angle δ. This process continues until rudder operation is conducted five times.

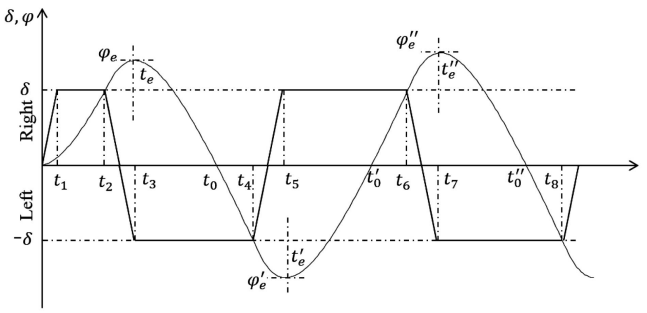

Figure 4 Characteristic curve of zig-zag manoeuvring test

In consideration of rudder angle error, to denote δ_r, Equation (8) can be written as Equation (13):

$$T\ddot{\varphi}+\dot{\varphi}=K(\delta+\delta_r) \tag{13}$$

Integrating Equation (13) from 0 to t_e, from 0 to t_e' and from 0 to t_e'', respectively.

$$\varphi(t_e)=K\int_0^{t_e}\delta dt+K\delta_r t_e \tag{14}$$

$$\varphi(t_e')=K\int_0^{t_e'}\delta dt+K\delta_r t_e' \tag{15}$$

$$\varphi(t_e'')=K\int_0^{t_e''}\delta dt+K\delta_r t_e'' \tag{16}$$

By combining Equations (15) and (16), K and δ_r can be obtained.

Then, integrate Equation (13) from 0 to t_0, from 0 to t_0' and from 0 to t_0'', respectively.

$$Tr(t_0)=K\int_0^{t_0}\delta dt+K\delta_r t_0 \tag{17}$$

$$Tr(t_0')=K\int_0^{t_0'}\delta dt+K\delta_r t_0' \tag{18}$$

$$Tr(t_0'')=K\int_0^{t_0''}\delta dt+K\delta_r t_0'' \tag{19}$$

Eventually, T is the average value calculated from Equation (17)-(19), respectively. And thus all of the

indices K and T, and rudder angle error δ_r can be obtained. Value K reflects the merits of the airboat turning ability. The bigger the value K is, the faster is the yaw rate of the airboat, and the smaller is the turning radius. Value T reflects the steering performance of the airboat. The smaller the value T is, the higher is the efficiency of the steering. In this case, the control time becomes shorter from steering the airboat to achieve the desired heading angle.

3 Results and discussion

According to the above theoretical analysis, a series of zig-zag maneuvering experiments were conducted using the agriculture airboat to obtain the indices K and T. The experiments were carried out in the experimental paddy field of Hokkaido University, Sapporo, Japan. Based on the obtained values of indices K and T, maneuvering simulations obtained by using Matlab (Version R2013a) were compared with field experiments.

3.1 Airboat zig-zag maneuvering experiments

Based on the ratio values of different rudder steering angles and heading angles, which is denoted as δ/φ, the conducted experiments were set to values of 15°/15°, 25°/25° and 35°/35°, respectively. The running speeds of the airboat were set to 1.2 m/s. The blades of the air propeller were kept at a constant angle of forward 30°. Figure 5 shows the real-time trace of the zig-zag maneuvering in different δ/φ states within 25 s.

In Figure 5, the solid line is the real-time heading angle obtained by the GPS compass while the dashed line is the real-time rudder angle through controlling the servo motor during zig-zag maneuvering. For calculating the Nomoto model indices K and T of the airboat, yaw rate was also required. Because of the field environmental disturbance and engine vibration, the high frequency noise was interfered into the yaw rate data obtained by IMU. The Savitzky-Golay smoothing filter[20] was used to filter the signal in this research. Figure 6 shows the original yaw rate data and processed data in different zig-zag maneuvering situation. The dashed line represents the original yaw rate data, while the solid line represents the processed data using the Savitzky-Golay smoothing filter.

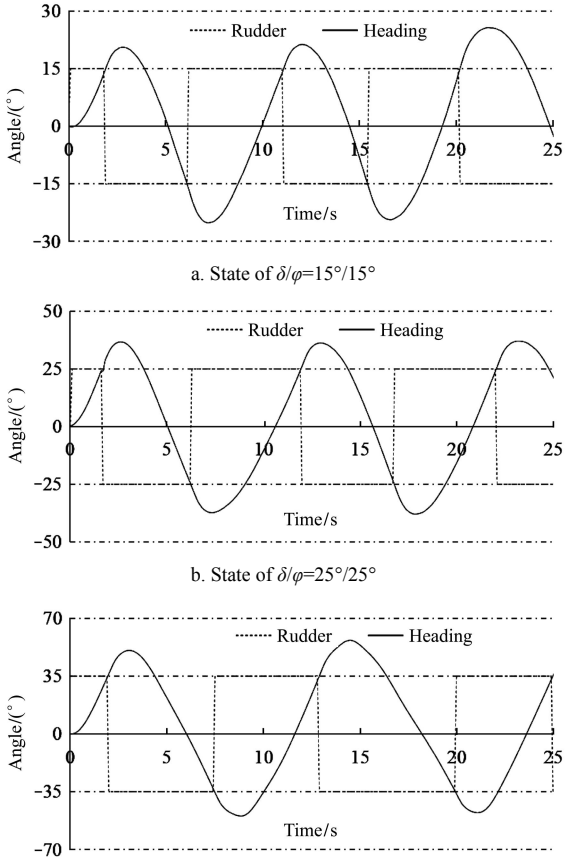

a. State of δ/φ=15°/15°

b. State of δ/φ=25°/25°

c. State of δ/φ=35°/35°

Figure 5 Real-time trace of rudder & heading value in different δ/φ states

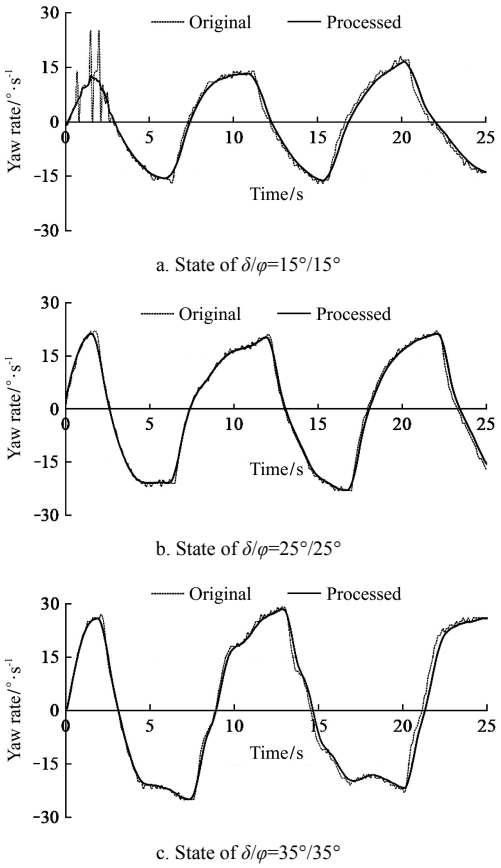

a. State of δ/φ=15°/15°

b. State of δ/φ=25°/25°

c. State of δ/φ=35°/35°

Figure 6 Real-time trace of yaw rate during zig-zag maneuvering experiments in different δ/φ states

From the zig-zag maneuvering data information in Figures 5 and 6, the Nomoto model indices K and T of the airboat in the states of 15°/15°, 25°/25° and 35°/35° respectively were calculated using the Equations (14)-(19). The calculated results of the Nomoto model indices K and T, and the corresponding rudder angle error δ_r are summarized in Table 2. It is shown that the indices K and T decreases along with the increase of rudder steering angle gradually.

Table 2 Summary of the Nomoto model indices K and T and rudder angle error δ_r in different δ/φ states

Indices	Zig-zag maneuvering states		
	15°/15°	25°/25°	35°/35°
K	1.349	1.006	0.825
T	1.950	1.854	1.312
δ_r/°	0.18	2.22	−1.83

3.2 Maneuvering simulation

Circular motion test is an experiment that changes the boat from rectilinear motion into circular motion under the effect of rudder operation. The turning circle is the 360° turning trajectory of the boat's gravity center under the condition of constant rudder angle and constant running speed. The turning circle radius is the main parameter for boat control. Hence, the circular motion maneuvering simulation is necessary for the agricultural airboat automatic control. To verify the obtained Nomoto model indices K and T, the index values in Table 2 were substituted into Equation (9). Then, the heading angle of the airboat could be obtained by integration using Equation (10). Assuming that the influence of water current, waves, wind and soil bulge in the paddy field can be neglected, the real-time position of the airboat can be simulated by Equations (11) and (12) when the rudder steering angle and the running speed are known. In the circular motion maneuvering simulations of this research, the speed of the airboat was set roughly to 1.2 m/s and the rudder was set to 15°, 25° and 35° respectively. Correspondingly, the paddy field experiments were also conducted under the same conditions of the above simulations in an approximate no-wind day. Right-hand circular motion test as an example was implemented. Figure 7 shows the simulated and experimental trajectories using rudder angles of 15°, 25° and 35°, respectively.

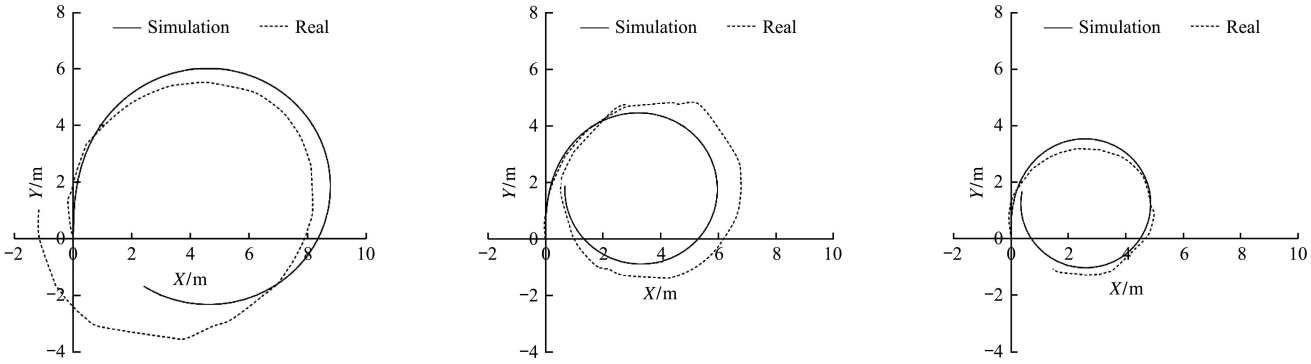

a. State of δ=15° b. State of δ=25 c. State of δ=35°

Figure 7 Right-hand circular trajectory comparison results for different rudder angles

In Figure 7, the solid circle is the simulated turning circular trajectory while the dashed circle trajectory shows actual circular motion test in paddy field. The trajectory data was obtained by using a total station (AP-L1A, Topcon) which was set on the embankment of the paddy field and the reflection prism fixed on the center of the airboat body. The total station functioned on an automatic target tracking mode and was used to record the position information in real time when the airboat runs in the paddy field. It could provide 10 mm+2 ppm mean squared error (MSE) measurement accuracy and the data refresh rate is 2 Hz. For comparing the circular turning effect, the least square method (LSM) was used to fit the turning circle of the simulation and the actual trajectory to achieve the turning radius. Table 3 summarizes the turning radius and radius error in different rudder angles. The turning radius of the actual circle is a little larger compared to the simulation at sub-meter level. The steerage is decreased in the actual environment because the water flow, wind action and soil bulge more or less exist in the field tests.

Table 3 Summary of the turning radius and radius error in different rudder angles

Turning radius/m	Rudder angle/(°)		
	15	25	35
Actual	4.49	3.20	2.39
Simulation	4.24	2.76	2.35
Difference	0.25	0.44	0.04

In order to fully verify the feasibility of the achieved Nomoto model indices, the sinusoidal running was also simulated by the zig-zag maneuver. Correspondingly, the simulations were conducted in the conditions of rudder angle of ±15°, ±25° and ±35° during 25 s respectively. The blades of the air propeller were also set to a constant angle of 30° forward, and the airboat speed was set to 1.2 m/s in the paddy field. Figure 8 shows the simulated and experimental trajectories for different rudder angles using Equations (11) and (12). Two full oscillation periods of sinusoidal running trajectory data were recorded within 25 s. In Figure 8a, the amplitude of the simulated trajectory is 1.44 m; the average amplitude of actual experimental trajectory is 1.53 m. It means that the amplitude error is 0.09 m. As an analogy, the amplitude errors are 0.54 m and 0.26 m when the rudder steering/heading ratio is 25°/25° and 35°/35° as shown in Figures 8b and 8c, respectively. Figure 9 shows the airboat speeds for different δ/φ states respectively.

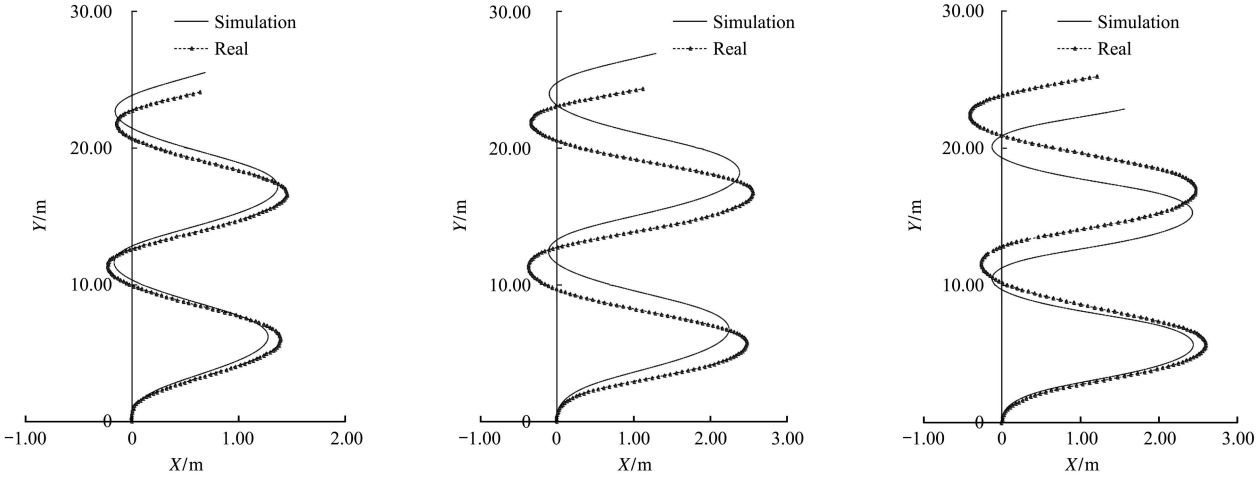

a. State of δ/φ=15°/15° b. State of δ/φ=25°/25° c. State of δ/φ=35°/35°

Figure 8 Sinusoidal running trajectory comparison results for different δ/φ states

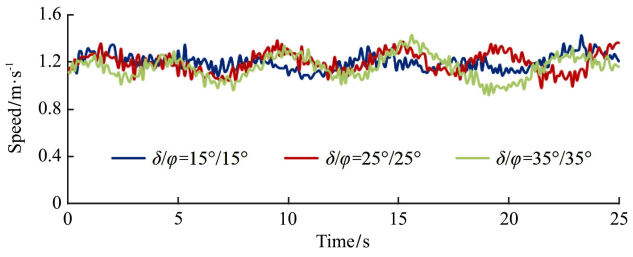

Figure 9 Speeds of Zig-zag test in paddy field for different δ/φ states

Based on Equation (9), the yaw rate comparison results between the simulations and field experiments in different rudder angles are shown in Figure 10. The solid line denotes the real experimental yaw rate, and the dashed line denotes the simulated yaw rate data.

As can be seen in Figure 10, the fluctuation range of the yaw rate in the simulation is very approximate with the performance in paddy field. Nevertheless, the phase difference between simulation and real test in each different rudder angles conditions exist, especially in the comparison of δ/φ=35°/35° condition. The reason is that disturbance of water flow and airflow effects on the airboat body were not considered when the maneuverability model was built. Although an approximate no-wind day was chosen, the breeze blew more or less from an uncertain direction occasionally. The speed cannot be easily kept at 1.2 m/s which is the constant value that was chosen in simulation as shown in Figure 9. The disturbed wind force which acted on the airboat can be divided into three force vectors in (o-xyz) direction, parallel to airboat body and perpendicular to airboat body. The wind force that is perpendicular to the airboat body in y direction can make the airboat change the predetermine course. It is adverse for keeping course track. In order to preliminarily explore the wind influence on this agriculture airboat shape, the

three-dimensional model shown in Figure 3 was built by using SolidWorks software based on the measured parameters. SolidWorks flow simulation tool was used to analyze the wind effect on airboat by using the effective environment parameters, e.g. air humidity was set as 70%, a hypothetic typical crosswind speed was set as 3 m/s under 0.1% turbulence intensity. Figure 11 illustrates the three main cross sections of airboat, noted as A, B and C respectively. Under the mentioned wind parameters, the crosswind effect on the three cross sections of the airboat are shown in Figure 12.

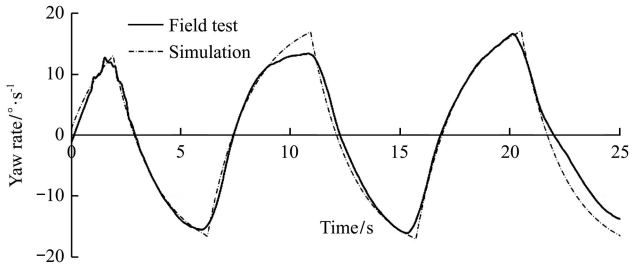

a. State of δ/φ=15°/15°

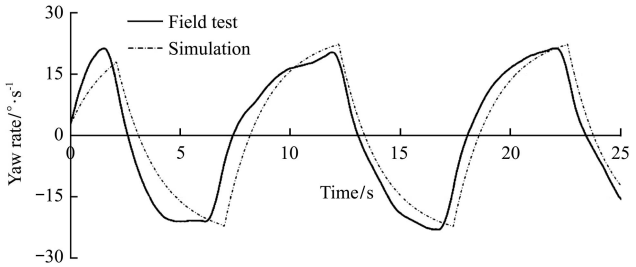

b. State of δ/φ=25°/25°

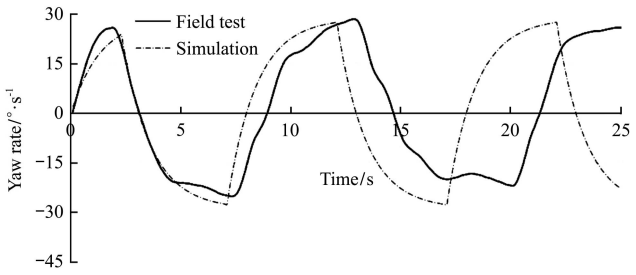

c. State of δ/φ=35°/35°

Figure 10 Yaw rate comparison results for different δ/φ states

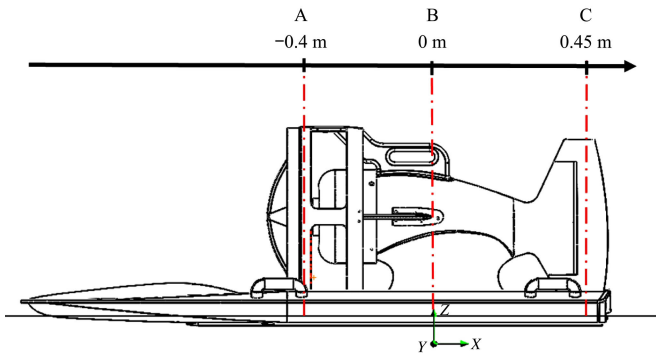

Figure 11 Three main cross sections of airboat

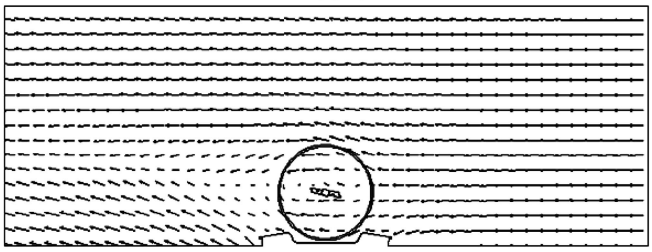

a. Wind effect on cross section A

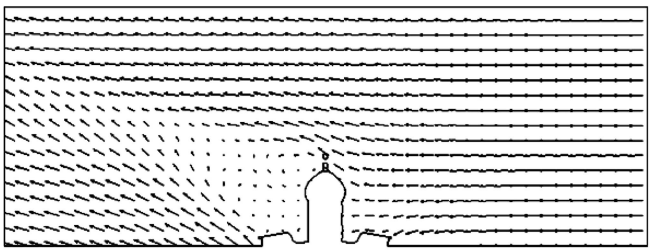

b. Wind effect on cross section B

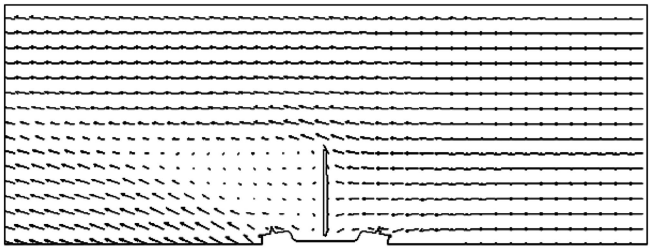

c. Wind effect on cross section C

Figure 12 Wind effect on the three main cross sections

Based on simulation and analysis, the maximum value of wind force on the right side of the airboat surface was 2.86 N. Furture work aims to advance more into the wind infulence analysis in the airboat maneuverability model. This is required to improve the control accuracy.

4 Conclusions

In this research, the unmanned airboat was modified from a radio-controlled air propeller boat to perform autonomous weeding and paddy growth monitoring in the paddy field. In order to achieve precise automatic control, the maneuverability of the airboat was derived based on the Nomoto model which describes the dynamics relationship between the rudder deflection and the airboat turning angular rate. The maneuverability indices of the Nomoto model were defined by adopting the zig-zag experiments. Matlab-based maneuvering simulations were conducted and compared with field experiments. Computer simulation and corresponding field tests verified the feasibility of the achieved maneuverability indices K and T. The comparison of the result shows that the trace error is at sub-meter level.

On account of the external disturbance including wind action, water flow and soil bulge, the comparison error has a tendency to increase over time. The wind influence was preliminarily simulated in a simple way. This challenge needs to be considered in depth in the future research.

Acknowledgements

The authors gratefully acknowledge the Biological Production Research Farm of Hokkaido University for providing the experimental paddy field.

[References]

[1] Airboat Afrika: What is an airboat. http://www.airboatafrika.com/about-airboats/. Accessed on [2016-10-13].

[2] Butterman E. A boat that walks on water. The American Society of Mechanical Engineers, 2013. https://www.asme.org/engineering-topics/articles/transportation/boat-that-walks-on-water. Accessed on [2016-10-13].

[3] Abdullah M O, Yek P N Y, Hamdan S, Junaidi E, Kuek P. An airboat for rural riverine transportation and mangrove marine environment applications. International Journal of Research and Reviews in Applied Sciences, 2010; 2(3): 211–222.

[4] Tuna G, Arkoc O, Gulez K. Continuous monitoring of water quality using portable and low-cost approaches. International Journal of Distributed Sensor Networks, 2013; 9(6): 1614–1617.

[5] James R. Winter survey by airboat on the frozen Mississippi river. Dpc Dredging & Port Construction, 1999; 26(2): 12.

[6] Nanson G C, Krusenstierna A V, Bryant E A, Renilson M R. Experimental measurements of river-bank erosion caused by boat-generated waves on the gordon river, Tasmania. River Research and Application, 1994; 9(1): 1–14.

[7] Dumment R. The use of airboat in ice and water rescue emergencies. Fire Engineering, 2004; 157(3): 113–126.

[8] Brouwer C, Prins K, Heibloem M. Irrigation water management: Irrigation scheduling. Training Manual, 1989; (4), FAO, Rome Italy.

[9] Sasaki Y, Kawano M. Current situations and outlook for Japanese paddy cultivating mechanization. North Rice, 2012; 42(6): 1–6. (in Chinese)

[10] Abkowitz M A. Measurement of hydrodynamic characteristic from ship maneuvering trials by system identification. Transactions of Society of Naval Architects and Marine Engineers, 1980; 88: 283–318.

[11] Ogawa A, Kasai H. On the mathematical model of maneuvering motion of ships. International Shipbuilding Progress, 1978; 25(292): 306–319.

[12] Fan S, Lian L, Ren P, Huang G. Oblique towing test and maneuver simulation at low speed and large drift angle for deep sea open-framed remotely operated vehicle. Journal of Hydrodynamics, 2012; 24(2): 280–286.

[13] Kenneth S M. Rotating arm model test facility. The American Society of Mechanical Engineers, 1981, October 14.

[14] Nomoto K. On the analysis of Z-manoeuvre tests. J.S.N.A. (Kansai), 1958; vol 92.

[15] Airboat specification. Yanmar Agri Japan Co., Ltd. http://www.yanmar.co.jp/hokuto/resale/contents.php?seq=149. Accessed on [2016-10-13].

[16] Hemisphere GPS V100 series user guide. http://hemispheregnss.com/Portals/0/technicaldocumentation/875-0174-000_b2%20(mnl,ug,v100%20series)_web.pdf. Accessed on [2016-10-13].

[17] VectorNav VN100 user manual. http://www.vectornav.com/docs/default-source/documentation/vn-100-documentation/UM001.pdf?sfvrsn=12. Accessed on [2016-10-13].

[18] Router WXR-2533DHP specification. Buffalo. http://buffalo.jp/product/wireless-lan/ap/wxr-2533dhp/. Accessed on [2016-10-13].

[19] Liu Y, Noguchi N, Yusa T. Development of an unmanned surface vehicle platform for autonomous navigation in paddy field. Proceedings of the 19th IFAC World Congress, Cape Town, South Africa, 2014 August 24-29. pp: 11553-11558.

[20] Savitzky A, Golay M J E. Smoothing and differentiation of data by simplified least squares procedures. Analytical Chemistry, 1967; 36(8): 1627–1639.